ResearchGate

See discussions, stats, and author profiles for this publication at: https://www.researchgate.net/publication/363846817

New archaeomagnetic directions from late Neolithic sites in Shandong province, China

Article *in* Geophysical Journal International · September 2022

DOI: 10.1093/gji/ggac381

CITATIONS
0

READS
54

11 authors, including:

Zheng Gong
Yale University
38 PUBLICATIONS **206** CITATIONS

SEE PROFILE

Stephen Victor
Yale University
9 PUBLICATIONS **27** CITATIONS

SEE PROFILE

Michael Corolla
Yale University
3 PUBLICATIONS **9** CITATIONS

SEE PROFILE

Jikai Ding
China University of Geosciences (Beijing)
26 PUBLICATIONS **542** CITATIONS

SEE PROFILE

Some of the authors of this publication are also working on these related projects:

Project Reconstructing West Africa in Proterozoic Supercontinents View project

Project Reconstructing marine redox conditions in Neoproterozoic time View project

All content following this page was uploaded by Zheng Gong on 01 October 2022.

The user has requested enhancement of the downloaded file.

New archaeomagnetic directions from late Neolithic sites in Shandong province, China

Qingzhu Wang [1,2,3,†], Zheng Gong [4,†,§], Stephen K. Victor [2,3], Michael Corolla [2,3], Anne P. Underhill [2], Roderick J. McIntosh [2,3], Hui Fang [1,5,6], Jikai Ding [4], Yichao Zhao [6,7], Xuexiang Chen [1,5,6], Yanbo Song [6,§]

[1] Institute of Cultural Heritage, Shandong University, Qingdao, Shandong, 266237, China

[2] Department of Anthropology, Yale University, 10 Sachem Street, New Haven, CT 06511, USA

[3] Yale Archaeomagnetism Laboratory, Yale University, 51 Hillhouse Avenue, New Haven, CT 06511, USA

[4] Department of Earth and Planetary Sciences, Yale University, 210 Whitney Avenue, New Haven, CT 06511, USA

[5] Joint International Research Laboratory of Environmental and Social Archaeology, Shandong University, Qingdao, Shandong 266237, China

[6] School of History and Culture, Shandong University, Jinan, Shandong 250100, China

[7] Shandong Provincial Institute of Archaeology, Jinan, Shandong 250002, China

[†] Equal contribution

[§] Corresponding authors: Zheng Gong (z.gong@yale.edu); Yanbo Song (songyb@sdu.edu.cn)

Summary

Archaeomagnetism provides important constraints to help us understand the past behavior of the geomagnetic field. For archaeologists, archaeomagnetic dating has become a potential supplement to traditional dating methods (e.g., radiocarbon dating). Although China has a long history with numerous archaeological discoveries, the collection of archaeomagnetic data remains scarce. In this paper, we provide new archaeomagnetic directions from four late Neolithic (c. 2000 BC) sites in Shandong province, China. After a careful characterization of magnetic mineralogy and a detailed alternating-field demagnetization of the oriented samples, a total of nine archaeomagnetic directions (each with both declinations and inclinations) were obtained, which fill the large gap at c. 2000 BC in the Chinese palaeomagnetic secular variation (PSV) curve. Combining these new results with previously published data, we updated the Chinese PSV curve for the last 7 kyr. We have compared the updated curve with several global geomagnetic models (e.g., pfm9k.1a, ARCH10k.1, CALS10k.1b). Comparisons show that the CALS10k.1b model does not yield a reasonable fit of the data, and the fit becomes worse for older intervals. This poor fit could be explained by the fact that the CALS10k.1b model consists of a large amount of sedimentary data. Therefore, the PSV pattern is difficult to determine due to the strong aliasing effect. On the contrary, the ARCH10k.1 model gives a much better fit than other models because its data are mostly from archaeological materials and the data are mainly from the Northern Hemisphere. The field intensity and PSV are potentially correlated, with a weak field corresponding to an enhanced PSV. However, due to the lack of data for certain time intervals, the proposed correlations need to be further tested. To explore if PSV exhibits longitudinal symmetric or latitudinal antisymmetric patterns like those of the geocentric-axial-dipole (GAD) model, we compiled and compared data from three East Asia countries (China, Korea, and Japan) and from four areas (East Asia, North

America, Europe and the Middle East, and Australia and New Zealand) of which the latitudes are between 30° and 40°. In the East Asia region, the PSV patterns shown in each dataset are consistent because of the geographic proximity of these three countries. However, when comparing the PSV curves from the four global areas, we suggest a potential declinational minimum between 0 AD and 2000 AD. Although further confirmation and investigation are needed, this declination minimum could be diachronous, sweeping from East Asia to Australia and New Zealand, and then North America. Future studies should focus on adding more reliable and precisely-dated data to better delineate the PSV trends. Archaeomagnetic dating is promising when a PSV curve can be continuously reconstructed.

Keywords

Archaeomagnetism, Palaeomagnetic secular variation, Rock and mineral magnetism, Palaeomagnetism, Asia

1. Introduction

Archaeological samples have been one of the most important archives for reconstructing the behavior of the ancient geomagnetic field on a millennial time scale (Brown et al. 2015, 2021). Archaeomagnetic data, together with sedimentary and volcanic records, have provided the most reliable constraints for regional and global geomagnetic field models published in the last few decades (e.g., Korte & Constable 2011; Nilsson et al. 2014; Constable et al. 2016; Hellio & Gillet 2018; Arneitz et al. 2019; Campuzano et al. 2019; Schanner et al. 2022). Compared with the igneous records, archaeomagnetic samples are much easier to date with high precision. Also, archaeomagnetic samples have a more straightforward mechanism of remanence acquisition than sedimentary records, and both the direction and absolute intensity of the ancient geomagnetic field can be obtained. However, major shortcomings of the archaeomagnetic dataset as of today are its insufficient number of data points and limited temporal and spatial coverage, with few data before 0 BC. Compilation from the GEOMAGIA50 v3.4 database shows that archaeomagnetic data distribution is highly skewed: a large portion of the data is from Europe (~60%) and very few data points (~7%) are from the southern hemisphere (Brown et al. 2015, 2021). This uneven distribution would certainly lead to a regionally biased global model. For example, China, where tens of thousands of archaeological discoveries have been made since the last century, has surprisingly scarce data (Cai et al. 2017). Most studies were conducted in the 1980s and even earlier when modern archaeomagnetic techniques and high-precision laboratory equipment had not been fully developed (e.g., Deng & Li 1965; Wei et al. 1980, 1981, 1983, 1984). After the study of Batt et al. (1998), archaeomagnetic research experienced a period of dormancy until the publications of Cai et al. (2015, 2016). Compared with palaeointensity data, even fewer directional data exist, which makes it more difficult to understand the palaeomagnetic secular variation (PSV) of the ancient geomagnetic field in China. In addition, archaeomagnetic dating has the potential to be one of the most important dating techniques for archaeological research. The most recent Chinese PSV curve constructed by Cai et al. (2016) is an encouraging start but still bears apparent gaps.

In this study, we report new archaeomagnetic directions from four late Neolithic (c. 2000 BC) sites in Shandong province, China (Fig. 1A). Archaeological and radiocarbon dating indicate that our new data fall within the data gaps of the Chinese PSV curve. Incorporating new data, we provide a more complete Chinese archaeomagnetic record for the last 7 kyr, which will be helpful to further refine regional and global geomagnetic field models. With more data available in the future, a robust PSV curve will greatly enhance the precision of archaeomagnetic dating as well.

2. Sample Background

2.1 Archaeological context and sampling

Our study was conducted in four archaeological sites in Shandong Province, China, specifically the Liangchengzhen, Sujiacun, Laiyang Dongqingbu, and Heze Qingqiu sites (Fig. 1A).

Liangchengzhen (LCZ) and Sujiacun (SJC) are both located in what is now the modern city of Rizhao, on the southeast coast of Shandong province. The LCZ site was one of two centers, and the SJC site was a third-tier center of a four-tier settlement system during the early Longshan period and a fourth-tier village during the middle Longshan period (2600-2200 BC) (Underhill et al. 2008; Fang et al. 2012; Chen et al. 2020; Song et al. 2020; Fang et al. 2022; also see Zhongmei Lianhe, 2016 for the first excavation at LCZ). The second phase of excavation at LCZ in 2018 by a Shandong University archaeology team uncovered 31 houses, 10 burials, and nearly 400 trash pits (Fig. S1). We took our samples in the summer of 2019 when the exposed features were preserved for exhibition. The samples (LCZ-1A, -1B) were collected from the hearth of F108, a nearly square house of 13.32 m^2 in size (Fig. S1). The circular hearth was located in the northeast corner of the house with well-consolidated red burned earth. Although the radiocarbon dates are not directly from our archaeomagnetic samples, the phases of the LCZ site are well defined and constrained by radiocarbon dating (Underhill et al. 2021). According to the excavation report, structure F108 was dated to the LCZ phases 2 to 3 (SDU & SDIA, 2021). Based on the seven Accelerator Mass Spectrometer (AMS) radiocarbon dates from macro-botanical remains from the previous excavation at LCZ (see Underhill et al. 2021), the LCZ phases 2 to 3 were dated to cal. 2290-1830 BC (calibrated dates from the beginning of phase 2 to the end of phase 3). We assigned this age to our LCZ archaeomagnetic samples.

We took the SJC samples in the summer of 2019 when the excavation of this site was taking place. During the excavation, 48 houses, 89 burials, and 207 trash pits were excavated, yielding thousands of various kinds of artifacts such as ceramic, stone, and jade (Song et al. 2020; SDU & SDIA, 2022; Fig. S1). Our samples were from the hearths of two houses (F24 and F29). Two sets of samples were collected from F24, a rectangular house of 25.5 m^2 in size (Fig. S1). During the excavation, three layers of floors were revealed. Each floor has a separate hearth located in the same location. Our samples were taken from the hearths of layer 2 (SJC-1A, -1B) and layer 3 (SJC-3A, -3B). Another set of samples (SJC-2A, -2B, -2C) was taken from the hearth of F29, a square house of 19.74 m^2 in size (Fig. S1). According to the newly published SJC excavation report (SDU & SDIA, 2022), the excavators of the SJC site identified three phases of occupation. The sampled house F24 is dated to the early phase of SJC, the calibrated radiocarbon date for which is cal. 2500-2340 BC (SDU & SDIA, 2022). The sampled house F29 is dated to the late phase of SJC, for which the calibrated radiocarbon date is cal. 2470-2300 BC (SDU & SDIA, 2022).

The Laiyang Dongqingbu site (LYDQB) is located ~13 km to the southwest of the modern city of Laiyang. The site is a Yueshi period settlement with a variety of houses. The two sets of samples (LYDQB-Z1-A, -Z1-B; LYDQB-Z2-A, -Z2-B) were taken from two hearths without associated houses (Fig. S1). There are no direct radiocarbon data from the site. Based on stratigraphy and typology, the dates of the two hearths can be constrained archaeologically to the Yueshi period, which is about 1800-1400 BC using a combination of relative (stratigraphy and ceramic typology) and absolute (radiocarbon dating) dating methods (see Luan & Wagner, 2009; Fang, 2013).

The Heze Qingqiu site (HQ) is located ~16 km southwest of the modern city of Heze. During the excavation in 2018, Longshan period (2600-1900 BC) and Yueshi period (1800-1400

BC) houses and trash pits, Shang period (1600-1050 BC) ritual remains, and Han period (208 BC-184 AD) burials were revealed. We took three sets of samples from the hearths of three houses (F1, F3, and F7; Fig. S2). Houses F1 and F3 are in the southern zone (Fig. S2). One set of samples was taken from F1, a rectangular house of 4.7 m^2 in size (Fig. S2). During the excavation, three layers of hearths were revealed, associated with the last three layers of the six consecutive floors (activity surfaces). We sampled the hearths at the top layer (HQ1-1) and the bottom layer (HQ1-2). The size and plan of F3 are unclear because only a small portion of the house was excavated. We took one sample (HQ3-1) from the hearth. House F7 is in the northern zone and was disturbed, but the hearth was well preserved. One sample (HQ7-1) was taken from the burned area. Based on ceramic typology, we assigned houses F1 and F3 to the Longshan period and house F7 to the Shang period. We used charred cereal grains to establish radiocarbon dates (see Section 3.1). The radiocarbon samples for houses F1 and F3 are from the associated culture layers (Unit T3927; Figs S2 and S3), and one radiocarbon sample (XA-23099) for house F7 is from the upper one of the two layers of soil deposits above the floor with the hearth we sampled (Fig. S2). The two layers were possibly formed to prevent humidity in the house and modify the previous floor, the one with the sampled hearth. Thus, the date of the radiocarbon sample should be close to that of the sampled hearth.

In total, 3 burnt features (7 samples) were collected from the SJC site, 1 burnt feature (2 samples) from the LCZ site, 2 burnt features (2 samples) from the LYDQB site, and 3 burnt features (4 samples) from the HQ site (Table 1).

2.2 Field techniques

Samples were chosen from burnt features *in situ*, that is, from hearths (Fig. 1). We looked for indications of the feature having been heated and cooled, using visual inspection (e.g., color and texture changes from heating) and sometimes employing a portable magnetic susceptibility meter (Bartington MS2 system). Because burnt earth samples are usually too friable for drilling, we used a bulk sampling technique similar to the plaster cap method of Thellier (1981) that maintains the orientation of the sample, which is essential for directional analysis. The selected bulk samples, usually up to about 10 cm in diameter, were isolated using typical nonmagnetic archaeological tools (Fig. 1B-D). Sample orientation was obtained in several steps. We first applied a layer of wet plaster about 1 cm thick on the top surface of the isolated sample (Fig. 1C). A square piece of plexiglass a bit larger than the sample was lightly oiled and placed on the plaster. Then a cross-test level was placed on the plexiglass. Pressing the plexiglass to make it level also leveled the moist plaster, providing a horizontal surface (Fig. 1B). Once the plaster was set, we removed the plexiglass cover, then indicated magnetic north on the sample by inscribing a north arrow on the top of the plaster, using a magnetic compass and awl. Those techniques provide the orientation of the sample, both azimuth and dip, necessary for archaeomagnetic analysis. Because of the field techniques used, the sample surfaces always have a magnetic 0° north azimuth and a dip of 0°. The samples were then removed to a depth of about 3 cm, covered with a consolidant, and transported to the lab.

2.3 Lab preparation

In the lab, the samples were cut into 8 cm^3 cubic specimens. Care was taken to preserve the azimuth and dip on each of the specimens. To prepare the oriented samples, we mounted the sample in a rectangular plastic box mold, making sure that the north arrow was parallel to the sides and that the surface was horizontal. Then the space around the sample was filled with plaster, creating a plaster block larger than the sample (Fig. 1E-G). The plaster block was then cut parallel to its sides, using a tile saw without lubrication, as water lubrication would dissolve unconsolidated burnt earth. Typically, five to six specimens from one sample were prepared for demagnetization, and leftover rock chips and powders were used for rock magnetic analyses. The sampling scheme is summarized in Figure S4.

3. Measurements

3.1 Radiocarbon dating

We analyzed four charred cereal grains from the HQ sites for their radiocarbon dates. The three samples are from layers 10, 11, and 14 of the excavation unit T3927 in the southern zone (Figs S2 and S3). Layers 10 and 11 are directly related to houses F1 and F3 and their hearths we sampled. In the northern zone, one radiocarbon sample provides a date for the sampled hearth of house F7 (Fig. S2). The carbonized grain samples were analyzed using the Ionplus MICADAS Accelerator Mass Spectrometer (AMS), of which the accuracy is better than 2‰ at the Xi'an AMS Center, Institute of Earth Environment, Chinese Academy of Sciences. The analysis follows the standard protocols. All ages were calibrated using the OxCal IntCAL20 model (Reimer et al. 2020) on the OxCal software (Bronk Ramsey et al. 2009).

3.2 Magnetic analyses

In order to characterize the magnetic mineralogy of the samples, we carried out a series of rock magnetic experiments on representative samples. Specifically, magnetic susceptibility versus temperature (k–T) experiments were performed using an AGICO Kappabridge KLY-4S susceptibility meter that is coupled with a CS3 temperature apparatus at the Yale Palaeomagnetism Facility. Samples were heated and cooled in an argon-gas environment. To better monitor magnetic mineralogical changes during the k–T experiments, each sample was measured in three temperature loops, first between 35 and 200°C, then between 35 and 400°C, and lastly between 35 and 700°C. In addition, hysteresis loops and backfield curves were obtained between -500 mT and 500 mT using a Princeton Measurement Corporation MicroMag 2900 Series alternating gradient magnetometer (AGM) at the Yale Archaeomagnetism Laboratory.

Oriented cubic specimens from each sample were demagnetized in three orthogonal directions step-by-step using an ASC Scientific D2000 alternating-field (AF) demagnetizer. After the measurement of natural remanent magnetization (NRM), AF demagnetization was performed following the steps of 2.5, 5, 7.5, 10, 15, 20, 25, 30, 35, 40, 50, 60, 80, 100, and 150 mT. For each step, remanent magnetization was measured using an AGICO JR-6A spinner magnetometer. The demagnetization and associated measurements were carried out in the two-layer Lodestar shielded room at the Yale Archaeomagnetism Laboratory. Palaeomagnetic analysis was conducted using Remasoft 3.0 software where data were plotted on the Zijderveld diagram (Zijderveld, 1967) and characteristic remanent magnetization (ChRM) of each sample was determined by principal component analysis (PCA, Kirschvink, 1980). Mean directions were calculated using Fisher spherical statistics (Fisher, 1953).

4. Results

4.1 Radiocarbon dating results

Radiocarbon dates of four charred cereal grains from the HQ sites (three from Unit T3927, and one from house F7) are presented in Figure 2. Specifically, cultural layer 14 is dated to 3860 ± 30

^{14}C year BP, which is calibrated to 2460-2200 cal. BC (95.4% probability), layer 11 is dated to 3700 ± 30 ^{14}C year BP, which is calibrated to 2200-1970 cal. BC (95.4% probability), and layer 10 is dated to 3510 ± 40 ^{14}C year BP, which is calibrated to 1950-1690 cal. BC (95.4% probability). Layers 10 and 11 are directly related to the houses and hearths where the archaeomagnetic samples were taken (Figs S2 and S3). As a result, we chose the start date of layer 11 and the end date of layer 10 to represent the age range of the archaeomagnetic samples from houses F1 and F3 (HQ1, HQ3), which is cal. 2200-1690 cal. BC. The sample from house F7 is dated to 3090 ± 25 ^{14}C year BP, which is calibrated to 1430-1280 cal. BC (95.4% probability). We assigned this age to the archaeomagnetic sample HQ7 (Fig. S2).

4.2 Magnetic mineralogy

Representative k–T curves for each site are shown in Figure 3. The k–T curves are reversible between 35 and 200°C. When the samples were heated up to 400°C, some minor changes were apparent when comparing the heating and cooling trajectories (Fig. 3). The broad decrease and the irreversibility of magnetic susceptibility between 300 and 400°C are indicative of the presence of maghemite (e.g., Deng et al. 2001; Liu et al. 2005; Gao et al. 2019) instead of Ti-rich magnetite. Between 35 and 700°C, the shapes of k–T curves are very different between the heating and cooling trajectories (Fig. 3). The largely reversible k–T curves below 400°C and irreversible k–T curves above 400°C suggest the original firing temperature must have been at least 400°C, and since then the samples appear not to have been heated above 400°C again or experienced much alteration. This interpretation is also supported by the experimental work of Hrouda et al. (2003). One common phenomenon is that all samples show a sharp decrease in magnetic susceptibility at ~585°C (Fig. 3), which is consistent with the Curie temperature of magnetite. On the heating curves, the increase of magnetic susceptibility between 480 and 550°C that precedes the Curie temperature is associated with mineralogical alternation. Compared with the heating curves, the higher cooling curves indicate some degree of mineralogical changes during heating even though the samples were heated in an argon-gas environment in order to minimize such reactions. New magnetite was likely made by the transformation of iron-bearing silicate minerals at high temperatures (e.g., Liu et al. 2020). Small tails on the heating curves between 600 and 700°C in some samples indicate the presence of hematite originally contained in the samples or newly formed from maghemite (Fig. 3). Overall, according to the k–T results, the magnetic mineralogy of the samples is dominated by magnetite, with a trace amount of maghemite and hematite.

The shape of the hysteresis loops suggests that after paramagnetic correction, all samples reach the saturation magnetization (M_s) well before 200 mT (Fig. 4). Coercivities (H_c) of the samples are between 3.6 mT and 10.2 mT, indicating a soft magnetic phase. The ranges of the H_c and the coercivity of remanence (H_{cr}) from the backfield curves fall within the typical values of magnetite (Peters & Dekkers, 2003). We calculated the ratio of saturation remanence (M_{rs}) and M_s, as well as the ratio of H_{cr} and H_c, and plotted them to qualitatively estimate the magnetic grain size (Day et al. 1977). Compared with the experimental results of Dunlop (2002), it appears that all samples lie within the pseudo-single domain (PSD) area (Fig. 5). Alternatively, this could also be explained by a mixed population of single-domain (SD) and multidomain (MD) grains (Dunlop, 2002). In either situation, these samples should be dominated by magnetic grains of the right sizes to genuinely record and preserve the ancient geomagnetic field information since the last time of firing.

4.3 Archaeomagnetic directions

Two components were revealed after the stepwise AF demagnetization. The first component can be isolated between NRM and 10 mT (Fig. 6) and is randomly distributed. This low-coercivity component is likely a viscous remanent magnetization that is acquired by large-sized, MD grains during transportation, storage, or preparation. After 10 mT, the samples usually show a clear decay-to-origin component up to 150 mT (Fig. 6), which is interpreted as the ChRM of the samples. The demagnetization coercivities are consistent with the range indicated by the hysteresis loops (Fig. 4). Some samples were not fully demagnetized at 150 mT (Fig. 6), which also points to the likely presence of high-coercivity magnetic minerals, such as hematite. Based on the demagnetization data and rock magnetic experiments, we interpreted that the ChRMs of the samples are dominantly carried by PSD magnetite.

To calculate the mean direction for each burnt unit, we used Fisher statistics (Fisher, 1953). Considering our sampling scheme (Fig. S4), we averaged the directions from specimens to get a sample mean. Since all the burnt units have three or fewer samples, we calculated the burnt unit means by including all the specimens from each individual unit. To be able to conveniently compare with other published archaeomagnetic data from China, we converted all directions to a reference point of 35°N, 105°E, following the convention of Cai et al. (2016). The directional data are shown in detail in Table 1.

5. Discussion

5.1 An updated Chinese PSV curve for the last 7 kyr

To provide a more continuous and complete PSV curve, we compiled all published archaeomagnetic directional data from China (Deng & Li 1965; Wei et al. 1980, 1981, 1983, 1984; Batt et al. 1998; Cai et al. 2016). A total of 42 declinational data points and 102 inclinational data points were in the Chinese dataset before this study, with ages ranging from c. 4500 BC to c. 1850 AD. Following Cai et al. (2017), we only included sites with full-directional data (both declination and inclination) to avoid potential orienting problems. In the end, a total of 42 data points were selected (Fig 7). By incorporating the new data from this study, we substantially expanded the size of the Chinese dataset. More importantly, our new results fill the large and critical data gap at 2500-1500 BC (Fig. 7). Our new data help better delineate the Chinese PSV curve, with moderately fluctuated declinations and inclinations between 2200 BC and 1800 BC (Fig. 7). Generally, the updated Chinese PSV curve shifts around the directions expected from the geocentric-axial-dipole (GAD) model in Figure 7. Declinations and inclinations do not vary simultaneously, nor do they vary at the same magnitude. For example, large declinational deviations occur at c. 1000 AD, c. 800 BC, and c. 3000 BC when inclinations don't show significant excursions. For inclinations, large deviations are apparent at c. 1500 AD and c. 100 BC, but the declinations seem to be consistent with the GAD model. In addition, declinations and inclinations show very fast variations between 1000 AD and 0 BC, but the variation rates become much slower and steady before 0 BC (Fig. 7). Furthermore, although gaps still exist, with more data available, trends postdating 2000 BC are better defined than older time intervals, and hence should be considered more reliable. However, compared with the European dataset, the Chinese PSV curve still needs to be further refined with more data in the future. Overall, our updated Chinese PSV curves are consistent with the curves proposed by Cai et al. (2017).

We have compared the updated Chinese PSV curve with a few global geomagnetic models that cover the same age range, for example, the pfm9k.1a (Nilsson et al. 2014), ARCH10k.1 (Constable et al. 2016), and CALS10k.1b models (Korte et al. 2011). In general, models pfm9k.1a and ARCH10k.1 could successfully capture the overall pattern of the updated Chinese PSV curve

(Fig. 7). However, model CALS10k.1b could only fit the younger quarter of the curve reasonably but exhibits large mismatches in the older segments (Fig. 7). One can observe that the variation of model CALS10k.1b is much flatter than the other two. Since model CALS10k.1b incorporates a large number of sedimentary data (Korte et al. 2011), the aliasing effect is significant, which could explain its flatness. Model pfm9k.1a also includes sedimentary data, but the aliasing effect was corrected by redistributing the weight given to different data types (Nilsson et al. 2014). Among the three models, ARCH10k.1 fits the updated Chinese PSV curve the best, which is likely because this model includes only archaeological data and is strongly biased towards the Northern Hemisphere (Constable et al. 2016), therefore, regionally it should give a more reasonable solution.

Field intensity curves were also plotted to explore the potential correlations between the palaeointensity and PSV (Fig. 7). We first attempted to see if large and fast PSV would correspond to a weak field. Around 300-0 BC, a shallowing trend of inclination and a westward drift of declination are noticed. However, palaeointensity values are not obviously lower than in other periods. On the contrary, we do not observe large PSV during an extremely weak field at 2200 BC shown in ArchInt_China.1a model (Cai et al. 2017). The low data resolution around that time interval in the current Chinese dataset could be one possible explanation. Another possibility is that the intensity decrease does not affect the PSV, which is possible in some geomagnetic simulation models (Brown & Korte, 2016). Alternatively, the robustness of this extremely weak field should be tested because it is only defined by one data point (Cai et al. 2017). Palaeointensity studies should be employed on samples of this age to see if this weak field at 2200 BC could be reproduced. Overall, based on the current data, there is no clear and straightforward correlation between PSV and palaeointensity.

5.2 Global mid-latitude PSV, and field symmetries

Under the GAD assumption, the geomagnetic field should exhibit longitudinal symmetry and latitudinal anti-symmetry. Therefore, it is worthwhile to explore these symmetries using regional and global archaeomagnetic datasets. Since the Chinese dataset has a mean latitude of 35°N, we compared the PSV curves from other mid-latitude regions. In order to incorporate a sufficient number of data points to produce meaningful PSV curves, we chose archaeomagnetic data between 30° and 40° latitude for the last 7 kyr. As a result, data show strong regional clustering (Fig. S5). Therefore, we binned the data into four regions, specifically, East Asia, North America, Europe and the Middle East, and Australia and New Zealand (Fig. S5). Firstly, we compared the data within the East Asia region, specifically the Chinese, Japanese, and South Korean datasets (Fig. 8). Due to the geographic proximity, some PSV patterns could actually be observed in multiple East Asian datasets. For instance, a declinational minimum around 800 AD, as well as an inclinational hump, is shown on Japanese and Chinese curves (Fig. 8). Broadly, the Chinese and Japanese palaeointensity curves are well matched to each other (Fig. 8). Although South Korea does not have enough data to produce comparable curves, there are no apparent incompatible directional and palaeointensity values. In terms of the comparison among the four regions globally, no clear longitudinally symmetric or latitudinal antisymmetric patterns could be easily observed because the data are sparse and unevenly distributed (Figs 9 and S5). However, we attempted to propose some potential patterns that should be further confirmed or rejected in the future. For example, between 0 AD and 2000 AD, a declinational minimum (i.e., a V-shaped declinational change) can be found in East Asia, North America, and Australia and New Zealand datasets show a similar shift in the magnitude of ~20° away from the GAD direction (Fig. 9). That indicates that there was a westward and then an eastward drift around that time. More interestingly, the minimum point of declinations is not synchronous. East Asia experienced this declinational drift transition the earliest, followed by Australia and New Zealand, and then North America (Fig. 9). Hypothetically, if this observation is confirmed by future studies, it would need to be explained why this declinational drift transition would be initiated in East Asia, sweeping across the Pacific Ocean and lastly arriving in North America. On the contrary, declinational data from the Europe and the Middle East show a maximum instead of a minimum around the same time interval (Fig. 9) which is not in agreement with the sweeping pattern mentioned above. Whether there was a strong local high-order field component beneath Europe and the Middle East, or whether the current observation was not robust needs to be further investigated. In terms of the inclination, a broad hump could be identified between 2000 BC and 0 BC in East Asia and Europe and the Middle East (Fig. 9). Data from Australia and New Zealand seem to suggest a period of low palaeointensity around the same time, which seems to be latitudinal antisymmetric to Northern Hemisphere. However, such a phenomenon is missing or yet to be revealed in North America. All these potential patterns in PSV and palaeointensity are worthwhile to look into to help us better understand the behavior of the geomagnetic field in a symmetric aspect, and any hypotheses regarding these patterns must be properly tested as more robust and well-dated archaeomagnetic data become available.

6. Concluding remarks

We have provided new archaeomagnetic directions from four late Neolithic sites in Shandong province, China, which fill the large gap in the Chinese dataset around 2000 BC. Incorporating our new data, we updated the Chinese PSV curve for the last 7 kyr. We have also compared our results with several global geomagnetic models. We found that the ARCH10k.1 model yields the best fit because the data this model uses are most relevant to our study area in terms of type and locality. On the contrary, the CALS10k.1b model fails to capture the overall pattern of the Chinese PSV curve, and the fit becomes worse in the older segment of the curve, which is likely due to the smoothing effect of the sedimentary data in the model. The relationship between palaeointensity and PSV is not straightforward, but during certain time intervals, low palaeointensity values correspond with larger variations in declinations and inclinations. We also compared the Chinese PSV curves with the curves of the other mid-latitudinal (30-40°N/S) regions to explore if the secular variation bears longitudinal symmetric or latitudinal antisymmetric patterns as predicted by the GAD assumption. PSV curves of China, Korea, and Japan show a good agreement for the last 7 kyr because these regions are geographically close to each other. However, data from the four widely-separated areas show several interesting features. One intriguing pattern is that a declinational minimum was observed between 0 AD and 2000 AD in the PSV curves of East Asia, North America, and Australia and New Zealand. However, this declinational minimum is diachronous, appearing in East Asia earliest, then Australia and New Zealand, and finally North America. Although further confirmation is needed, this sweeping pattern could shed light on the short-term variation of the geodynamo. So far, sparsity and uneven distribution of the data are the main barriers to drawing clear conclusions. These issues should be addressed in future studies. As summarized by Brown et al. (2021), global archaeological data still face several major challenges including uncertainties in age constraints, biased data distribution, and sparse data in certain time periods. Global geomagnetic models also heavily rely on robust archaeomagnetic data to give a holistic and precise representation of PSV patterns through space and time. Currently, archaeomagnetic dating is still at its early stage, especially for places in which the PSV curve is still not well established (e.g., China or the Southern Hemisphere). By combining both directional and intensity data and integrating the constraints from archaeological features, reasonable ages could potentially be assigned. Statistical tests such as Monte Carlo simulations could also be very helpful for properly assigning uncertainties in archaeological dating.

7. Data Availability Statement

Raw palaeomagnetic, and rock magnetic data underlying this article are available in the GitHub repository (https://github.com/zheng-gong-pmag/Shandong-Archaeomagnetism.git), and are also archived on Zenodo (https://doi.org/10.5281/zenodo.7113280). Global geomagnetic models and archaeomagnetic data are available in the GEOMAGIA50 v3.4 Database (https://geomagia.gfz-potsdam.de).

Acknowledgments

We thank Yu Dong, Yang Gao, Xinyu Wang, and Karol Stoker for field assistance. Zheng Gong was supported by the Yale Graduate Student Fellowship. Qingzhu Wang and Stephen K. Victor were supported by the Yale University Albers-Coe-Hazard funds for field excavation. Yanbo Song was supported by the Shandong University multidisciplinary research and innovation team of young scholars (2020QNQT018). The radiocarbon dating for the excavation unit T3927 from the Heze Qingqiu site was funded by the National Social Science Foundation of China (General Program 20BKG003) to Xuexiang Chen. The Yale Council on East Asian Studies supported Anne P. Underhill's involvement in the 2019 field season. The Columbia University Department of East Asian Languages and Cultures supports Qingzhu Wang during manuscript preparation. We thank David Evans for allowing us to use the facilities in the Yale Palaeomagnetism Laboratory, and Gary Crawford (University of Toronto) for sharing unpublished information regarding the AMS dates. Tinghong Zhou (University of Rochester) is thanked for her help with interpreting rock magnetic data. We are grateful to the former President of the Shandong University, Liming Fan, for her continuous support of the Yale-Shandong University collaborative project on archaeomagnetic dating. Careful and detailed comments provided by Andy Biggin, Catherine Batt, and an anonymous reviewer helped to improve the quality of the manuscript.

References

Arneitz, P., Egli, R., Leonhardt, R., & Fabian, K. (2019). A Bayesian iterative geomagnetic model with universal data input: Self-consistent spherical harmonic evolution for the geomagnetic field over the last 4000 years. *Physics of the Earth and Planetary Interiors*, 290, 57-75.

Batt, C., Meng, Z., & Nöel, M. (1998). New archaeomagnetic studies near Xi'an, China. *Archaeometry*, 40(1), 169-175.

Bronk Ramsey, C. (2009) Bayesian analysis of radiocarbon dates. *Radiocarbon*, 51(1) 337-360.

Brown, M. C., Donadini, F., Korte, M., Nilsson, A., Korhonen, K., Lodge, A., ... & Constable, C. G. (2015). GEOMAGIA50. v3: 1. General structure and modifications to the archeological and volcanic database. *Earth, Planets and Space*, 67(1), 1-31.

Brown, M. C., & Korte, M. (2016). A simple model for geomagnetic field excursions and inferences for palaeomagnetic observations. *Physics of the Earth and Planetary Interiors*, 254, 1-11.

Brown, M. C., Hervé, G., Korte, M., & Genevey, A. (2021). Global archaeomagnetic data: The state of the art and future challenges. *Physics of the Earth and Planetary Interiors*, 318, 106766.

Cai, S., Chen, W., Tauxe, L., Deng, C., Qin, H., Pan, Y., ... & Zhu, R. (2015). New constraints on the variation of the geomagnetic field during the late Neolithic period: Archaeointensity results from Sichuan, southwestern China. *Journal of Geophysical Research: Solid Earth*, 120(4), 2056-2069.

Cai, S., Tauxe, L., Deng, C., Qin, H., Pan, Y., Jin, G., ... & Zhu, R. (2016). New archaeomagnetic direction results from China and their constraints on palaeosecular variation of the geomagnetic field in Eastern Asia. *Geophysical Journal International*, 207(2), 1332-1342.

Cai, S., Tauxe, L., Paterson, G. A., Deng, C., Pan, Y., Qin, H., & Zhu, R. (2017). Recent advances in Chinese archeomagnetism. *Frontiers in Earth Science*, 5, 92.

Campuzano, S. A., Gómez-Paccard, M., Pavón-Carrasco, F. J., & Osete, M. L. (2019). Emergence and evolution of the South Atlantic Anomaly revealed by the new paleomagnetic reconstruction SHAWQ2k. *Earth and Planetary Science Letters*, 512, 17-26.

Chen, X. X., Yu, S. Y., Wang, Q., Cui, X., & Underhill, A. P. (2020). More direct evidence for early dispersal of bread wheat to the eastern Chinese coast ca. 2460-2210 BC. *Archaeological and Anthropological Sciences*, 12(10), 1-12.

Constable, C., Korte, M., & Panovska, S. (2016). Persistent high paleosecular variation activity in southern hemisphere for at least 10000 years. *Earth and Planetary Science Letters*, 453, 78-86.

Day, R., Fuller, M., & Schmidt, V. A. (1977). Hysteresis properties of titanomagnetites: grain-size and compositional dependence. *Physics of the Earth and Planetary Interiors*, 13(4), 260-267.

Deng, C. L., Zhu, R. X., Jackson, M. J., Verosub, K. L., & Singer, M. J. (2001). Variability of the temperature-dependent susceptibility of the Holocene eolian deposits in the Chinese loess plateau: a pedogenesis indicator. *Physics and Chemistry of the Earth, Part A: Solid Earth and Geodesy*, 26(11-12), 873-878.

Deng, X. H., & Li, D. J. (1965). The geomagnetic field in Peking region and its secular variation during the last 2000 years. *Acta Geophysica Sinica*, 14, 181-196.

Dunlop, D. J. (2002). Theory and application of the Day plot (M_{rs}/M_s versus H_{cr}/H_c) 1. Theoretical curves and tests using titanomagnetite data. *Journal of Geophysical Research: Solid Earth*, 107(B3), EPM-4.

Fang, H., Underhill, A., Feinman, G., Nicholas, L., Luan, F., Yu, H., Cai, F. (2012). Report of the systematic archaeological regional survey in the coastal region of Southeastern Shandong (in Chinese). Beijing: Wenwu Press.

Fang, H. (2013). The eastern territories of the Shang and Western Zhou: Military expansion and cultural assimilation. In: Underhill, A. (Ed), *A Companion to Chinese Archaeology*. Wiley-Blackwell, pp. 473-494.

Fang, H. Underhill, A. P., Feinman, G. M., Nicholas, L., M., Luan, F., Yu, H. (2022). Development of Complex Societies in Southeastern Shandong, China. Yale University Publications in Anthropology Number 97. Yale University Press, New Haven.

Fisher, R. A. (1953). Dispersion on a sphere. *Proceedings of the Royal Society of London. Series A. Mathematical and Physical Sciences*, 217(1130), 295-305.

Gao, X., Hao, Q., Oldfield, F., Bloemendal, J., Deng, C., Wang, L., ... & Guo, Z. (2019). New high-temperature dependence of magnetic susceptibility-based climofunction for quantifying paleoprecipitation from Chinese loess. *Geochemistry, Geophysics, Geosystems*, 20(8), 4273-4291.

Hellio, G., & Gillet, N. (2018). Time-correlation-based regression of the geomagnetic field from archeological and sediment records. *Geophysical Journal International*, 214(3), 1585-1607.

Hrouda, F., Müller, P., & Hanák, J. (2003). Repeated progressive heating in susceptibility vs. temperature investigation: a new palaeotemperature indicator? *Physics and Chemistry of the Earth, Parts A/B/C*, 28(16-19), 653-657.

Kirschvink, J. (1980). The least-squares line and plane and the analysis of palaeomagnetic data. *Geophysical Journal International*, 62(3), 699-718.

Korte, M., & Constable, C. (2011). Improving geomagnetic field reconstructions for 0-3 ka. *Physics of the Earth and Planetary Interiors*, 188(3-4), 247-259.

Liu, Q., Deng, C., Yu, Y., Torrent, J., Jackson, M. J., Banerjee, S. K., & Zhu, R. (2005). Temperature dependence of magnetic susceptibility in an argon environment: implications for pedogenesis of Chinese loess/palaeosols. *Geophysical Journal International*, 161(1), 102-112.

Liu, C., Wang, W., & Deng, C. (2020). A new weathering indicator from high-temperature magnetic susceptibility measurements in an Argon atmosphere. *Geophysical Journal International*, 221(3), 2010-2025.

Luan, F., & Wagner, M. (2009). The chronology and basic development sequence of archaeological cultures in the Haidai Region. In: Wagner, M., Luan, F., & Tarasov, P. (Eds.), Chinese Archaeology and Palaeoenvironment I: Prehistory at the Lower Reaches of the Yellow River: The Haidai Region. Mainz: Verlag Philipp von Zabern, pp. 1-15.

Nilsson, A., Holme, R., Korte, M., Suttie, N., & Hill, M. (2014). Reconstructing Holocene geomagnetic field variation: new methods, models and implications. *Geophysical Journal International*, 198(1), 229-248.

Peters, C., & Dekkers, M. J. (2003). Selected room temperature magnetic parameters as a function of mineralogy, concentration and grain size. *Physics and Chemistry of the Earth*, 28, 659-667.

Reimer, P. J., Austin, W. E., Bard, E., Bayliss, A., Blackwell, P. G., Ramsey, C. B., ... & Talamo, S. (2020). The IntCal20 Northern Hemisphere radiocarbon age calibration curve (0-55 cal kBP). *Radiocarbon*, 62(4), 725-757.

Schanner, M., Korte, M., & Holschneider, M. (2022). ArchKalmag14k: A Kalman-Filter Based Global Geomagnetic Model for the Holocene. *Journal of Geophysical Research: Solid Earth*, 127(2), e2021JB023166.

SDU (Shandong University), & SDIA (Shandong Provincial Institute of Archaeology) (2021). Report for the 2018 excavation at the Liangchengzhen site, Rizhao, Shandong (in Chinese). *Kaogu* (10), 16-37.

SDU (Shandong University), & SDIA (Shandong Provincial Institute of Archaeology) (2022). Report for the 2019 excavation at the Sujiacun site, Rizhao, Shandong (in Chinese). *Kaogu* (8), 3-24.

Song, Y., Dong, Y., & Wu, X. (2020). Longshan Culture houses and burials discovered at Sujiacun, Rizhao, Shandong (in Chinese). *China Relics Newspaper*. 2022-01-03 (008).

Thellier, E. (1981). Sur la direction du champ magnétique terrestre, en France, durant les deux derniers millénaires. *Physics of the Earth and Planetary Interiors*, 24(2-3), 89-132.

Underhill, A. P., Feinman, G. M., Nicholas, L. M., Fang, H., Luan, F., Yu, H., & Cai, F. (2008). Changes in regional settlement patterns and the development of complex societies in southeastern Shandong, China. *Journal of Anthropological Archaeology*, 27(1), 1-29.

Underhill, A. P., Cunnar, G. E., Luan, F., Crawford, G., Yu, H., Fang, H., ... & Wu, H. (2021). Urbanization in the eastern seaboard (Haidai) area of northern China: Perspectives from the late Neolithic site of Liangchengzhen. *Journal of Anthropological Archaeology*, 62, 101288.

Wei, Q. Y., Li, D., Cao, G. Y., Zhang, W. X., & Wang, S. P. (1980). Archaeomagnetic research of Jiangzhai relic, Neolithic epoch. *Acta Geophysica Sinica*, 23, 403-414.

Wei, Q. Y., Li, T. C., Chao, G. Y., Chang, W. S., & Wang, S. P. (1981). Secular variation of the direction of the ancient geomagnetic field for Loyang region, China. *Physics of the Earth and Planetary Interiors*, 25(1), 107-112.

Wei, Q. Y., Li, T. C., Chao, G. Y., Wang, S. P. & Wei, S. F. (1983). Results from China, in Geomagnetism of Baked Clays and Recent Sediments, Vol. 324, pp. 138-150, eds. Creer, K. M., Tucholka, P. & Barton, C. E., Elsevier.

Wei, Q. Y., Li, D. J., Cao, G. Y., Zhang, W. X. & Wang, S. P. (1984). The wandering path of virtual geomagnetic pole during the last 6000 years, *Acta Geophysica Sinica*, 27, 562-572.

Zijderveld, J. D. A. (1967). A. C. demagnetization of rocks: analysis of results. In: Collison, D. W., Creer, K. M. & Runcorn, S. K. (eds) Methods in Paleomagnetism. Elsevier, Amsterdam, 254-286.

Zhongmei Lianhe Kaogu Dui, Eds. (Luan, F., Underhill, A., Yu, H., Fang, H., Cai, F., Wang, F, Cunnar, G.) (2016). Liangchengzhen: 1998-2001 excavation report, four volumes (Liangchengzhen—1998-2001 in Chinese). Beijing: Wenwu Press.

Table 1 Summary of sample locations, ages, and archaeomagnetic directions. Slat = site latitude, Slon = site longitude, Dec = declination, Inc = inclination, Dec_r = relocated declination, Inc_r = relocated inclination, α95 = radius of 95% confidence cone, k = precision parameter, n = number of specimens included in mean calculation, N = total number of specimens. Burnt unit means are marked in bold and italic fonts. Data are relocated to the center of China (35°N, 105°E).

Site	Slat (°N)	Slon (°E)	Burnt unit	Sample	Age (BC)	Dec (°)	Inc (°)	Dec_r (°)	Inc_r (°)	α_{95} (°)	k	n/N
Sujiacun	35.496	119.588	SJC-1	SJC-1A	2500-2340	11.6	54.5			7.6	102.3	5/5
Sujiacun	35.496	119.588		SJC-1B	2500-2340	10.6	52.1			3.6	452.7	5/5
			Mean SJC-1			***11.1***	***53.3***	***10.1***	***50.4***	***3.6***	***181.0***	***10/10***
Sujiacun	35.496	119.588	SJC-2	SJC-2A	2470-2300	359.0	53.3			5.2	313.2	4/5
Sujiacun	35.496	119.588		SJC-2B	2470-2300	5.8	48.7			9.7	90.7	4/5
Sujiacun	35.496	119.588		SJC-2C	2470-2300	1.3	51.6			3.6	452.7	5/5
			Mean SJC-2			***2.0***	***51.3***	***0.9***	***50.4***	***3.0***	***191.9***	***13/15***
Sujiacun	35.496	119.588	SJC-3	SJC-3A	2500-2340	15.4	61.5			8.2	88.0	5/5
Sujiacun	35.496	119.588		SJC-3B	2500-2340	5.9	55.2			5.0	235.2	5/5
			Mean SJC-3			***10.2***	***58.5***	***10.8***	***56.0***	***4.8***	***102.3***	***10/10***
Liangchengzhen	35.571	119.572	LCZ-1	LCZ-1A	2210-1880	358.5	46.6			2.5	937.8	5/5
Liangchengzhen	35.571	119.572		LCZ-1B	2210-1880	0.8	48.6			0.7	11950.3	5/5
			Mean LCZ-1			***359.7***	***47.6***	***357.7***	***47.2***	***1.4***	***1191.7***	***10/10***
Laiyang Dongqingbu	36.933	120.587	***LYDQB-Z1***	LYDQB-Z1-A	1900-1500	***358.2***	***44.0***	***355.0***	***42.4***	***3.1***	***610.2***	***5/5***
Laiyang Dongqingbu	36.933	120.587	***LYDQB-Z2***	LYDQB-Z2-A	1900-1500	***4.4***	***52.7***	***3.0***	***49.7***	***2.2***	***1210.7***	***5/5***
Heze Qingqiu	35.164	115.279	HQ1	HQ1-1a	2200-1690	355.8	49.5	354.8	50.1	12.7	95.3	3/6
Heze Qingqiu	35.164	115.279		HQ1-2	2200-1690	1.8	59.8	3.1	59.4	8.1	90.2	5/5
			Mean HQ1			***359.2***	***55.9***	***359.5***	***55.8***	***6.6***	***70.8***	***8/11***
Heze Qingqiu	35.164	115.279	***HQ3***	HQ3-1	2200-1690	***359.0***	***58.1***	***359.8***	***58.0***	***3.7***	***428.6***	***5/5***
Heze Qingqiu	35.164	115.279	***HQ7***	HQ7-1	1430-1280	***9.8***	***47.4***	***8.2***	***45.6***	***5.7***	***181.2***	***5/5***

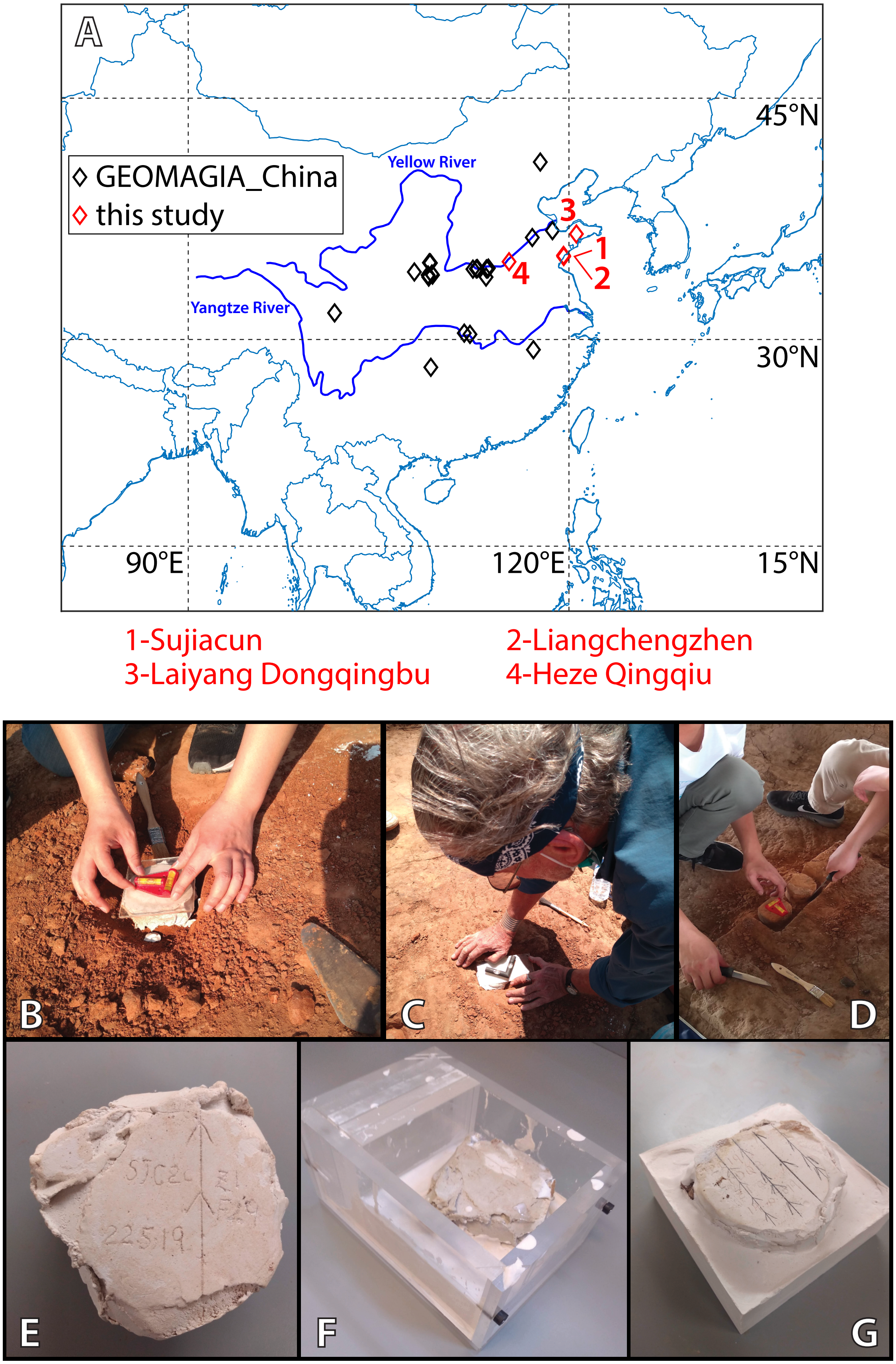

Figure 1 (A) Locations of archaeomagnetic directional data from China. Black diamonds show published data compiled from the GEOMAGIA50 v.3.4 database. Red diamonds show the locations of 4 sites in this study. (B-G) Field and lab photos show the sample collection and preparation procedures.

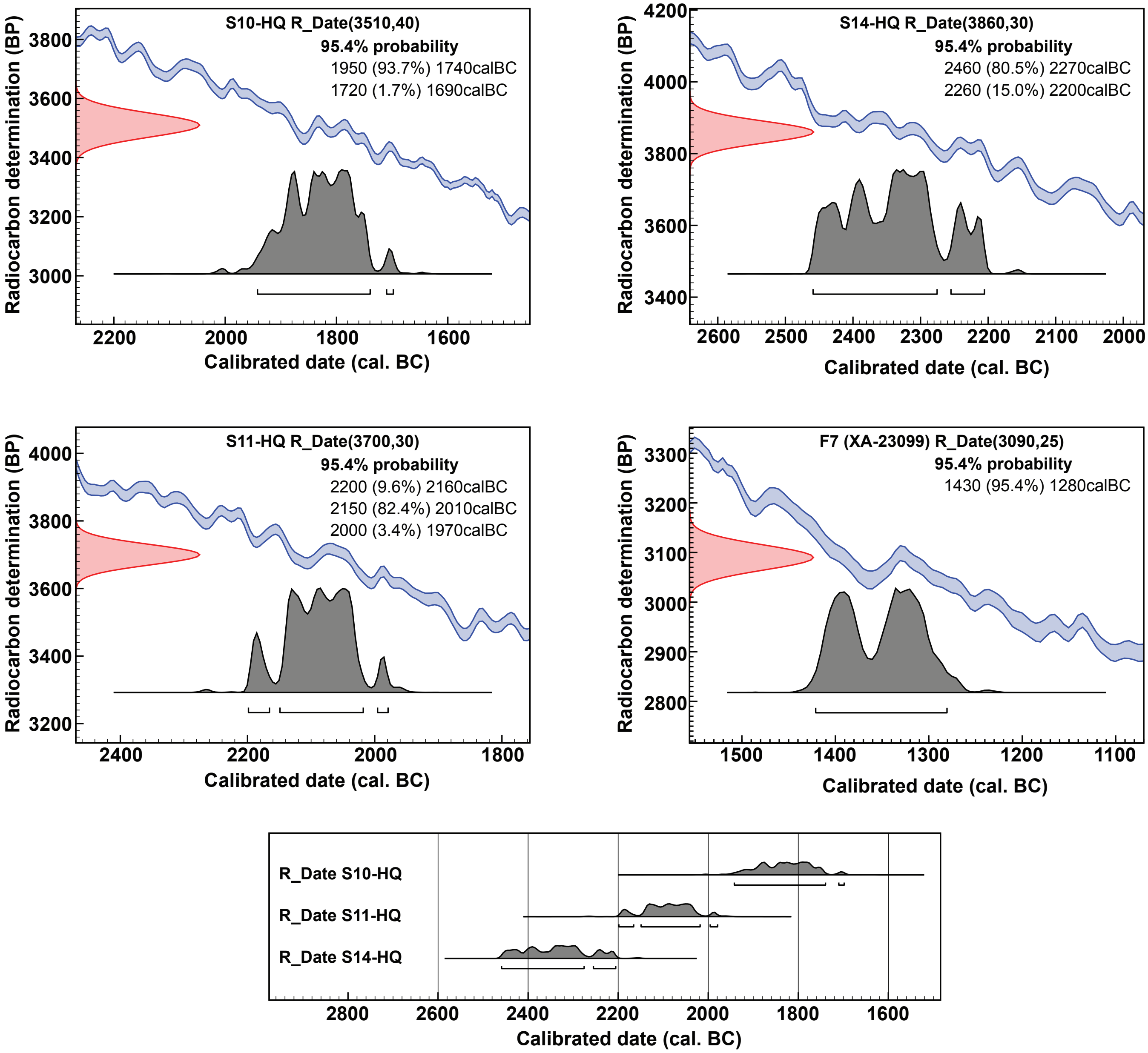

Figure 2 Radiocarbon ages from the Heze Qingqiu site. Sample locations are shown in supplementary figures 2 and 3.

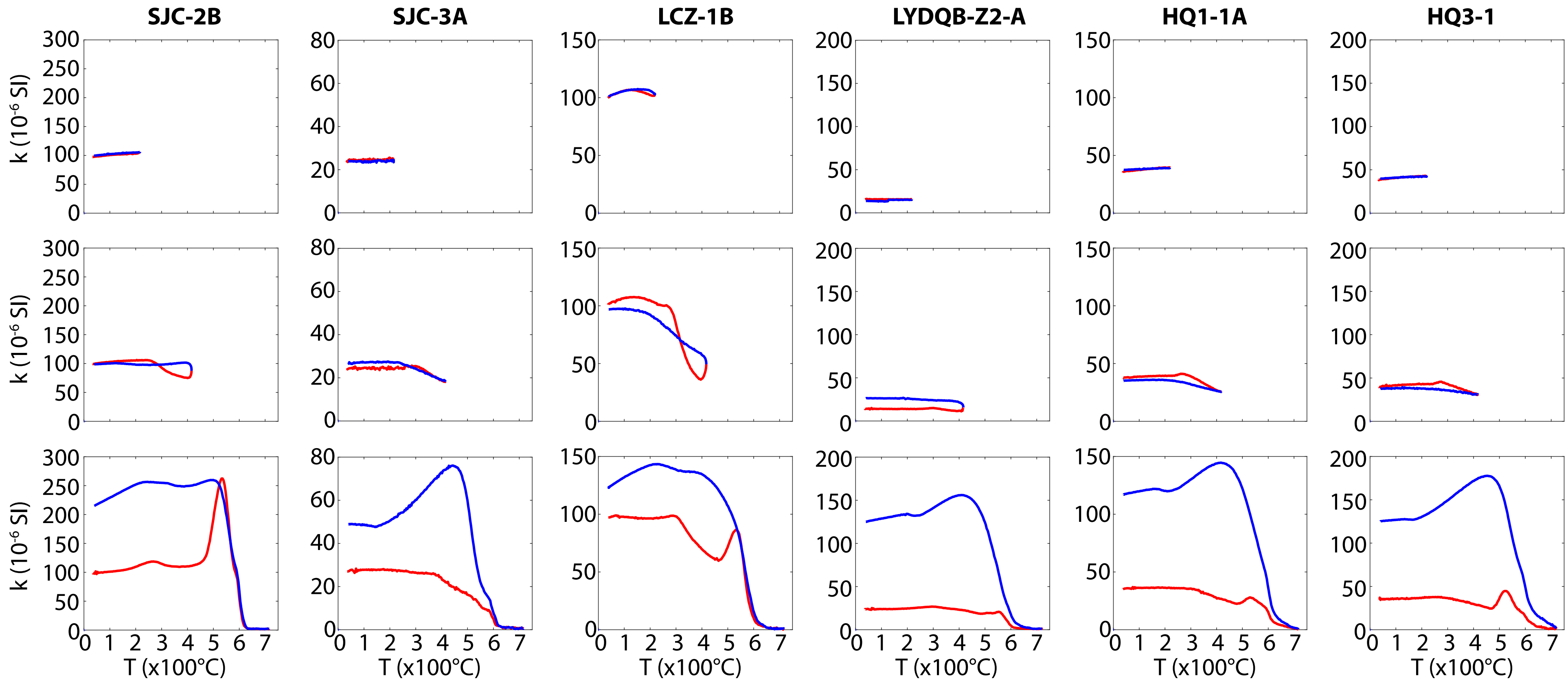

Figure 3 Representative magnetic susceptibility versus temperature (k–T) curves. Red and blue lines indicate heating and cooling trajectories, respectively.

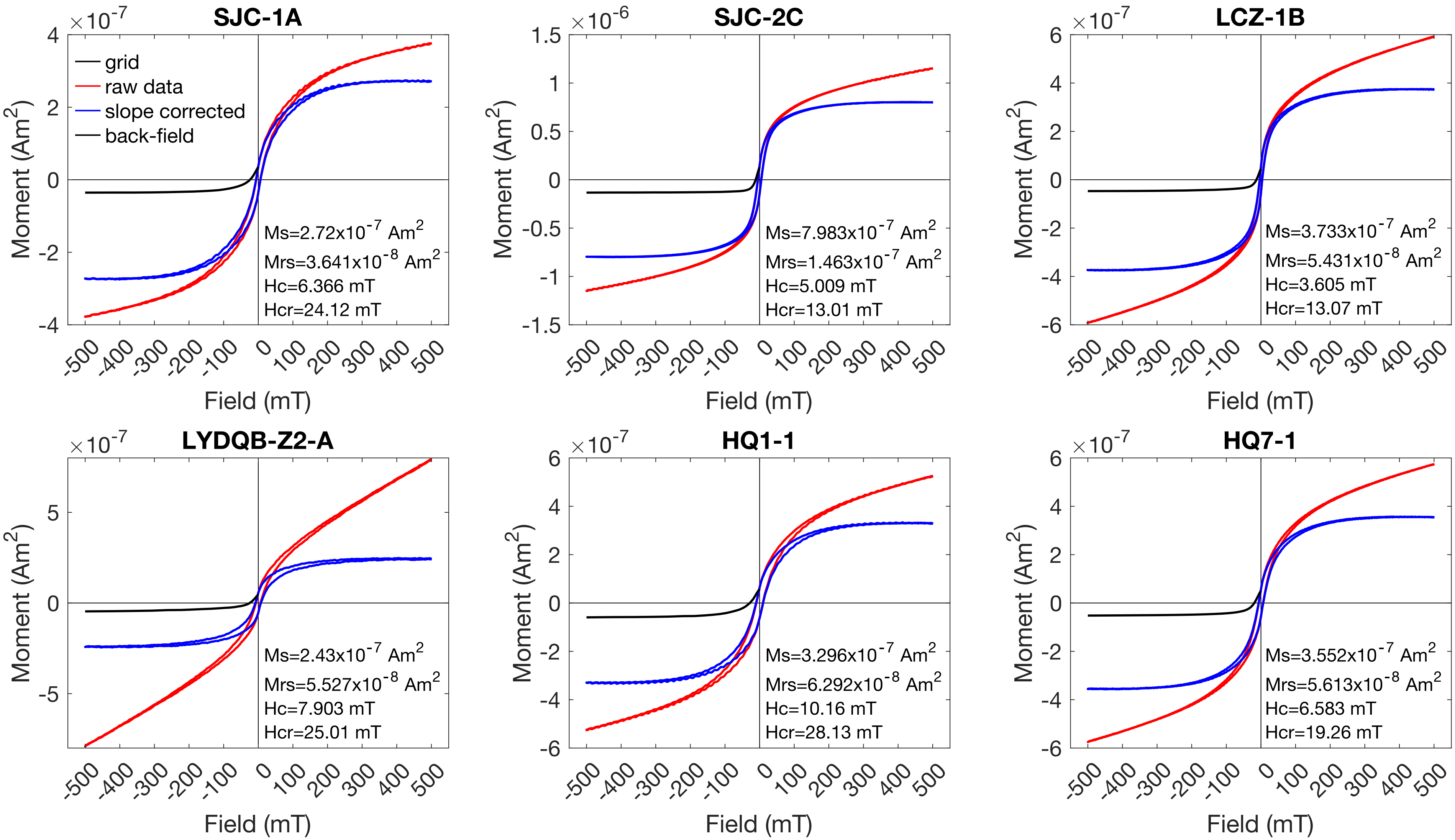

Figure 4 Representative hysteresis loops. Red solid lines are raw data, blue lines are data after paramagnetic correction, and black lines are back-field curves.

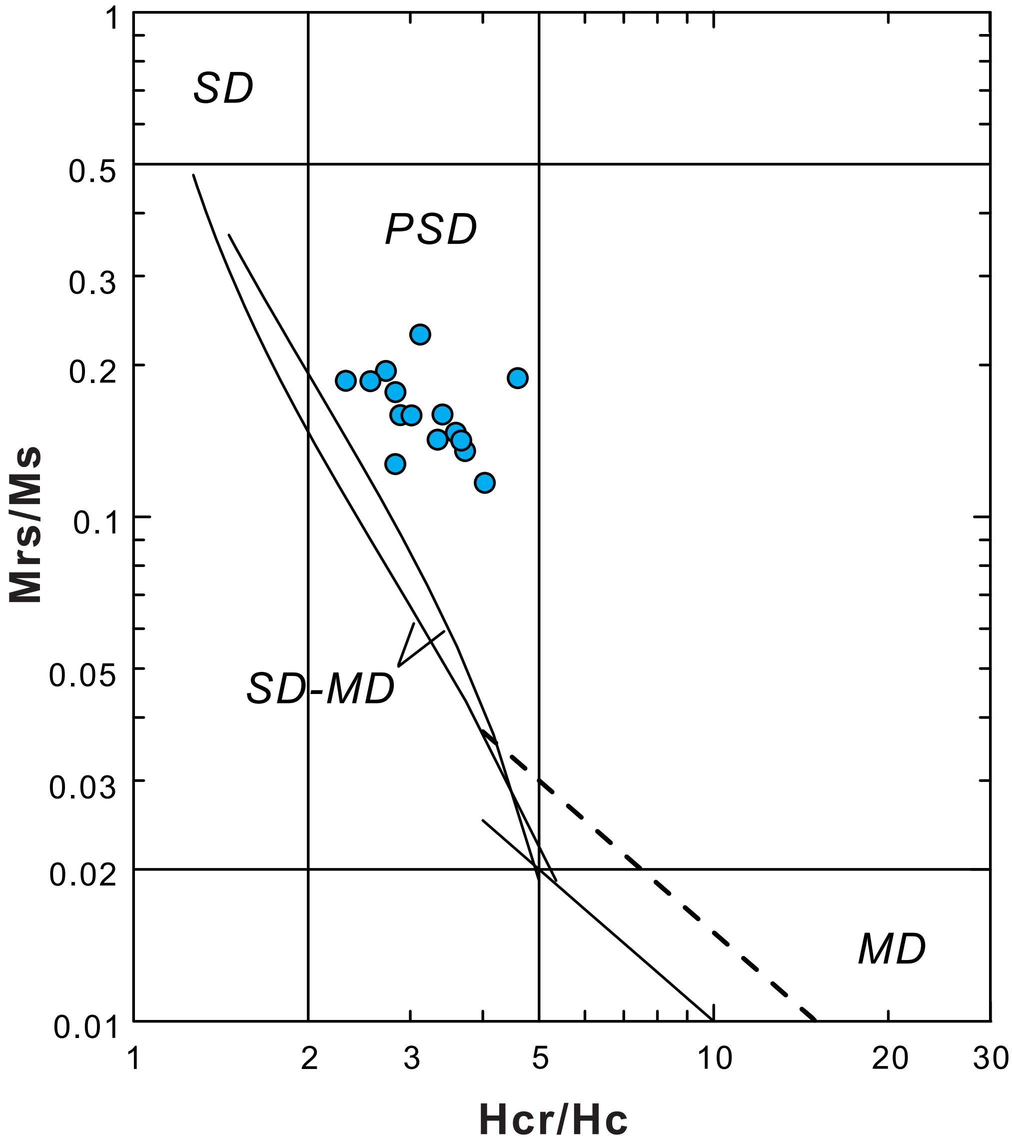

Figure 5 Day plot. Domain divisions and mixing lines are from Dunlop (2002). SD = single domain, PSD = pseudo-single domain, MD = multidomain.

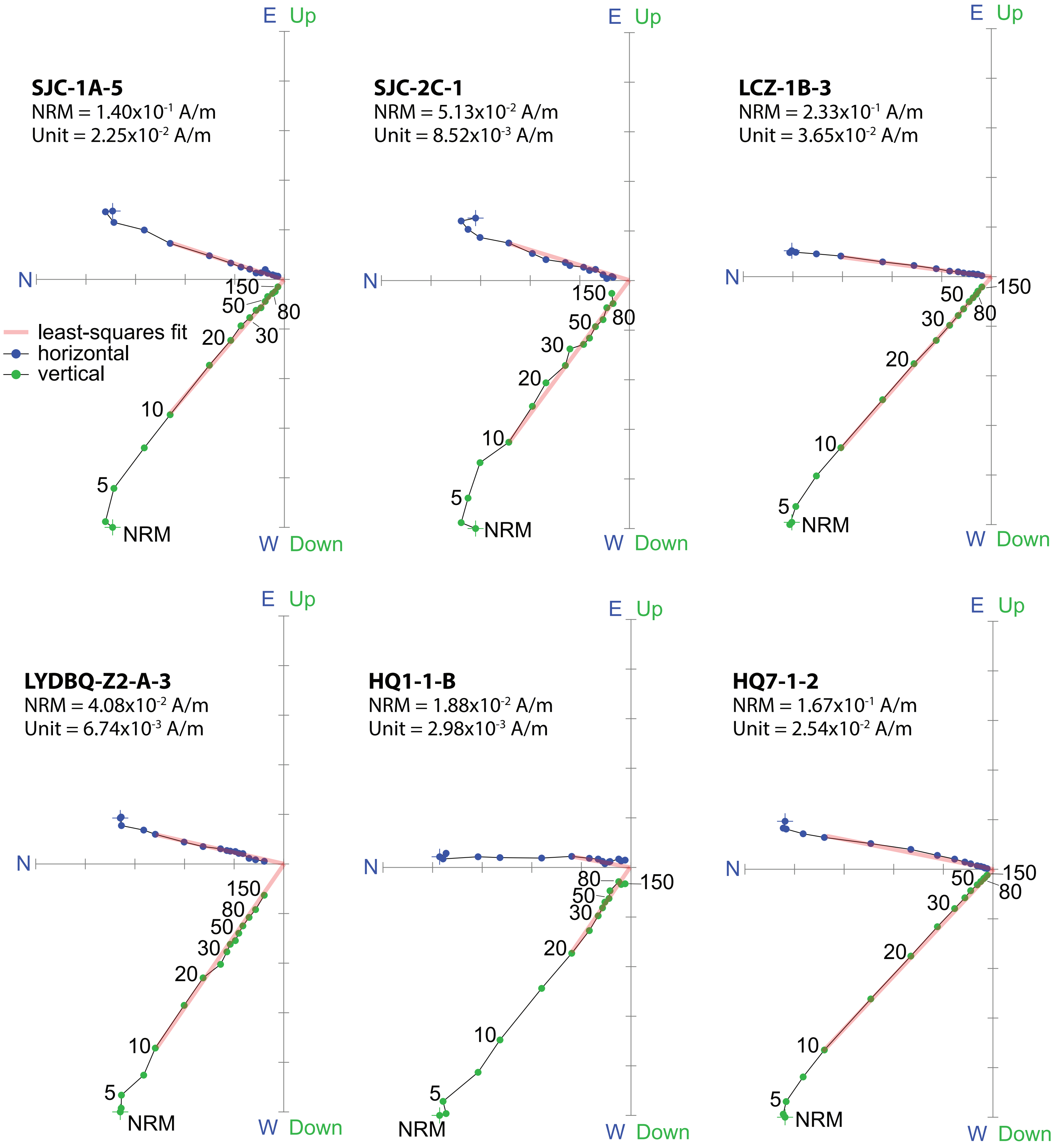

Figure 6 Representative alternating-field demagnetization data are shown by the Zijderveld diagrams. Blue and green dots are horizontal and vertical projections, respectively. Natural remanent magnetization (NRM) is marked by a cross on top of the point. Peak lines are the least-squares fits. Numbers show the alternating-field demagnetization steps in mT unit.

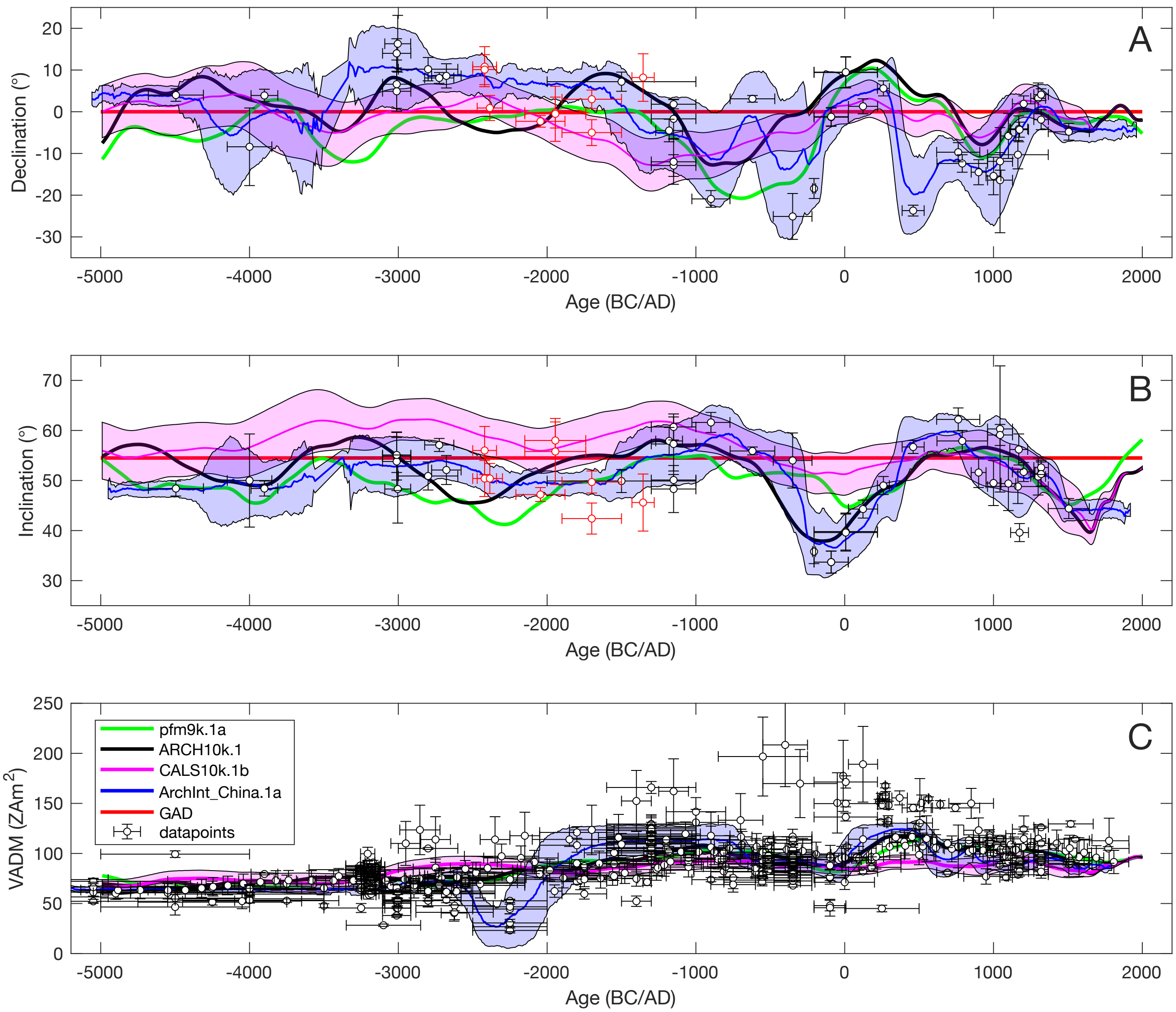

Figure 7 Palaeosecular variation (PSV) and virtual axial dipole moment (VADM) palaeointensity curves of China for the last 7 kyr. Black circles are published data from China. Red circles are data from this study. Green, blue, magenta, and black lines are direction and intensity predictions at 35°N, 105°E from four geomagnetic field models with corresponding error envelopes. Red lines show the expected declination and inclination at 35°N, 105°E based on the GAD model.

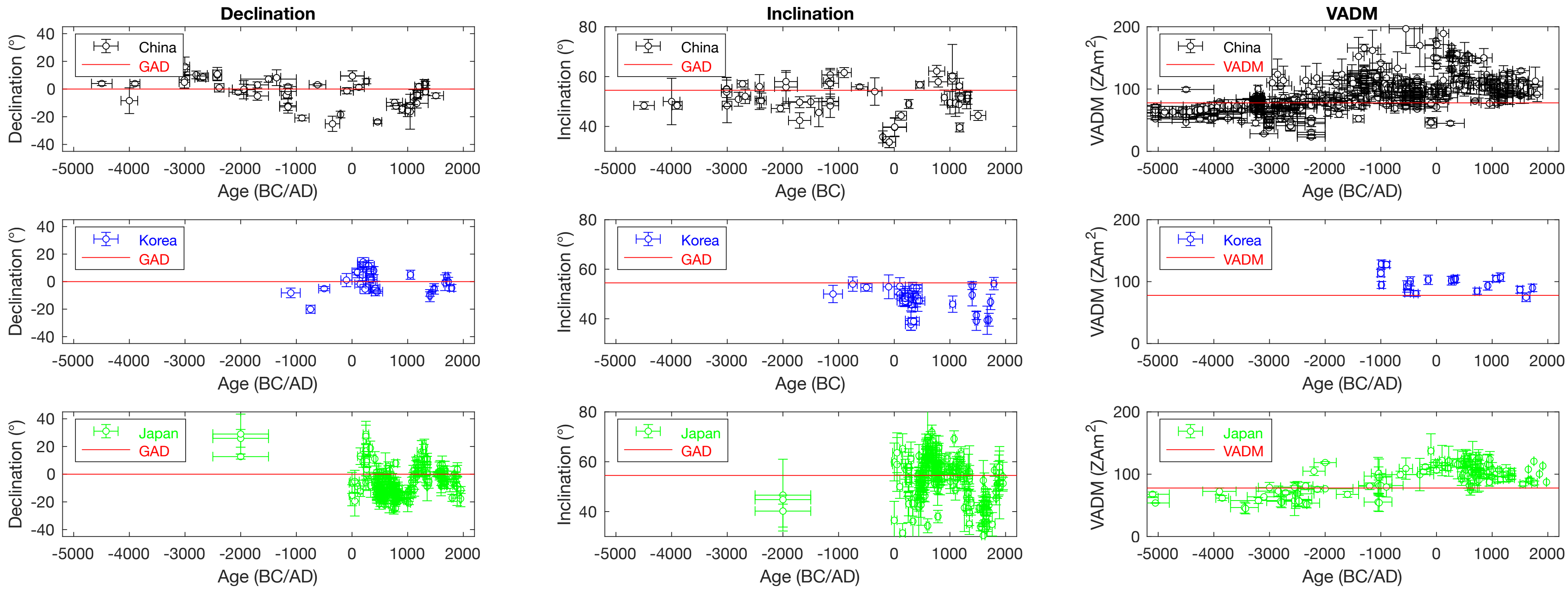

Figure 8 Palaeosecular variation (PSV) and virtual axial dipole moment (VADM) palaeointensity curves from three East Asian countries for the last 7 kyr. Data are relocated to 35°N, 120°E. Red lines are expected directions at 35° latitude based on the GAD model.

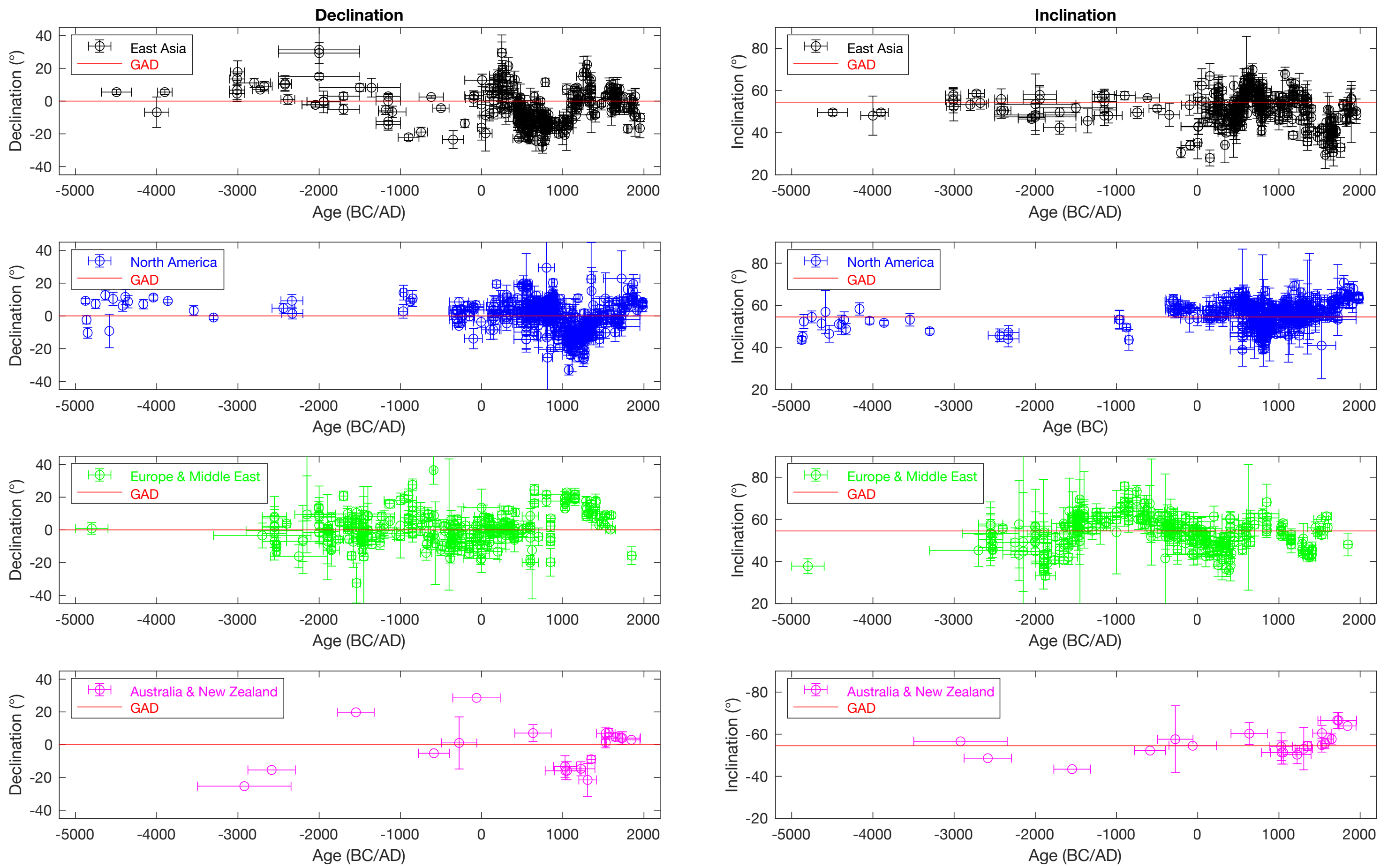

Figure 9 PSV curves from four mid-latitudinal regions for the last 7 kyr. Data from East Asia are relocated to 35°N, 120°E, data from North America are relocated to 35°N, 270°E, data from Europe and the Middle East are relocated to 35°N, 30°E, and data from Australia and New Zealand are relocated to 35°S, 150°E. Red lines are expected directions at 35° latitude based on the GAD model.

View publication stats